Supporting Information

Li et al. 10.1073/pnas.1312455111

SI Materials and Methods

Animals. Long–Evans rats [postnatal day (P)19–P36; both sexes] were used.

Whisker Deprivation. D row (D1–D6) and γ-whiskers on the right side were trimmed to the skin every other day under isoflurane anesthesia. Whiskers were allowed to regrow for 3 d before in vivo recording, and whisker deflection was delivered through the regrown stub. For 1 d of deprivation, trimmed whiskers were glued back to the stub for recording. Control animals were littermates that underwent anesthesia and handling (sham trimming). For slice physiology experiments, whiskers were plucked instead of trimmed.

In Vivo Recordings. Rats were anesthetized with urethane (1.5 g/kg induction, 10% supplemental injections as needed). The skull was thinned over left primary somatosensory cortex for intrinsic signal optical imaging (ISOI). Whisker deflection was delivered by piezos using standardized ramp–hold–return deflections [2°, 4-ms ramp, 62.5 mm/s (550°/s) velocity, 100- or 500-ms hold for single-unit or whole-cell recordings, respectively]. All whiskers (control and deprived rats) were deflected 3 mm from the face. Cortical representations of one D-row whisker and two immediately adjacent C- and E-row whiskers were mapped under red light illumination (630 nm) using a Dalsa 1M60 camera as described previously (1). Response area was defined as the region with >0.015% change in intrinsic signal.

Extracellular recordings were made with tungsten electrodes (3.5 MΩ) targeted at the center of mass of a D-whisker ISOI response area. Recordings (0.5- to 8-kHz band pass, 3,000× gain, 32-kHz digitization, 12-bit resolution) were made at spontaneously active sites every ∼70 μm from 168 to 800 μm below the pia. Spike sorting was performed offline, and laminar location was inferred from recording depth [layer 2/3 (L2/3): 150–600 μm below pia; L4: 600–900 μm] (2). Spontaneous firing in a 100-ms prestimulus window was subtracted from whisker-evoked responses. Electrolytic lesions were made in L4 to mark recording sites, which were recovered in cytochrome oxidase-stained tangential sections to determine recording locations relative to barrel boundaries. Sites in septa or inappropriate columns were excluded.

Whisker-evoked local field potentials were recorded with tungsten electrodes (2-kHz low pass, 100× gain) at 400 (L2/3) and 800 μm (L4) below the pia simultaneously with most single-unit recordings. Current source density analysis was performed in one experiment (Fig. S3*A*), in which whisker-evoked local field potentials were measured with a linear silicon probe (A1x16-3mm-100-413-A16; Neuronexus) positioned in the D1 column with the top recording site at the pia (0-μm depth). Frequency-dependent phase shifts caused by analog hardware filters were corrected offline (FPAlign; Plexon Inc.). The current source density was calculated as the second spatial derivative using a finite difference formula and spatially smoothed using a (0.25, 0.5, 0.25) triangle filter (3).

In Vivo Whole-Cell Recording. The craniotomy was perfused with Ringer's solution [119 mM NaCl, 26.2 mM $NaHCO_3$, 11 mM D-(+)-glucose, 1.3 mM $MgSO_4$, 2.5 mM KCl, 1 mM NaH_2PO_4, 2.5 mM $CaCl_2$ bubbled with 95% O_2/5% CO_2 (vol/vol), pH 7.30, 290 mOsm]. L2/3 neurons (depth = 273–590 μm) were patched using standard blind patching techniques (4, 5), with pipettes 20–30° off radial. Internal solution contained cesium and N-(2,6-dimethylphenylcarbamoylmethyl)triethylammonium (QX-314) bromide to block voltage-gated K^+ and Na^+ conductances and 1,2-bis(o-aminophenoxy)ethane-N,N,N′,N′-tetraacetic acid (BAPTA) to inhibit Ca^{2+} gated conductances (88 mM CsOH, 88 mM D-gluconic acid, 20 mM Hepes, 5 mM tetraethylammonium chloride (TEACl), 2.8 mM NaCl, 0.4 mM EGTA, 0.3 mM Na_3GTP, 4 mM MgATP, 10 mM Na_2-phosphocreatine, 5 mM BAPTA, 25 mM QX-314, pH 7.20). Resting potential was measured immediately after break-in. Vhold values were corrected for a 10 mV liquid junction potential. Series resistance (Rseries) and input resistance (Rinput) were measured in each sweep from a double exponential fit to the membrane current transient evoked by a hyperpolarizing voltage step (−5 mV). Rseries was not corrected.

In each cell, the principal whisker (PW) was identified as the whisker that evoked the largest PW-evoked postsynaptic current (wPSC) at −70 mV. The PW matched ISOI map location for 21 of 25 cells in control animals (P23–P36), confirming the accuracy of ISOI targeting. The wPSCs (mean of 12–75 repetitions) were recorded at five holding potentials (−90, −68, −40, 0, and +30 mV) in response to standardized whisker deflections. Cells were accepted for analysis if (*i*) wPSCs reversed at Vhold ≥ 0 mV; (*ii*) Rseries was <30 MΩ; (*iii*) Rseries, Rinput, and holding current (Ihold) changed <30% during the recording period (0.5–2 h); and (*iv*) the current–voltage (I–V) relationship at the peak of the wPSC was linear. Recording location was verified histologically for a subset of cells (n = 11) by marking the penetration track with ink. All 11 cells were localized to the cortical column corresponding to the PW.

Estimation of Synaptic Conductance. Whisker-evoked excitatory synaptic conductance [Gex(t)] and inhibitory synaptic conductance [Gin(t)] were estimated using standard methods (6, 7). First, the total synaptic conductance [Gtotal(t)] and reversal potential [Erev(t)] at each time point t were determined using data from the five holding potentials by linear fit of the equation

$$\mathrm{Isyn}(t) = \mathrm{Gtotal}(t) \times (\mathrm{Vhold}(t) - \mathrm{Erev}(t)),$$

where Isyn(t) is the synaptic current measured in response to whisker deflection and Vhold(t) is the holding potential adjusted for ohmic loss through Rseries. Gtotal excludes resting conductance. Second, Gex(t) and Gin(t) were calculated by the equations (6)

$$\mathrm{Gin}(t) = \mathrm{Gtotal}(t) \times (\mathrm{Eex} - \mathrm{Erev}(t))/(\mathrm{Eex} - \mathrm{Ein}) \text{ and}$$

$$\mathrm{Gex}(t) = \mathrm{Gtotal}(t) - \mathrm{Gin}(t),$$

where Eex and Ein are the reversal potentials for excitation and inhibition (0 and −68 mV, respectively, as determined in L2/3 pyramidal cells in primary somatosensory slices). Conductances were analyzed in the window of 0–77 ms poststimulus, where I–V curves were most consistently linear. Gex and Gin were constrained to be nonnegative (7).

Slice Physiology. Rats were anesthetized with isoflurane, and the brain was quickly removed in cold cutting solution [75 mM sucrose, 85 mM NaCl, 25 mM D-(+)-glucose, 25 mM $NaHCO_3$, 4 mM $MgSO_4$, 2.5 mM KCl, 1.25 mM NaH_2PO_4, 0.5 mM $CaCl_2$ bubbled with 95% O_2/5% CO_2 (vol/vol), pH 7.20]. Cortical slices (400 μm) were cut from the left hemisphere in the across-row plane (50° to coronal from sagittal, 10° down angle), and therefore each slice contained one barrel from the A–E whisker rows (8, 9). Slices were incubated in oxygenated normal Ringer's solution (119 mM NaCl, 26.2 mM $NaHCO_3$, 11 mM D-(+)-glucose,

1.3 mM $MgSO_4$, 2.5 mM KCl, 1 mM NaH_2PO_4, 2.5 mM $CaCl_2$, pH 7.30) for 30 min at 30 °C and 0.5–6 h at room temperature before recording.

Whole-cell recordings were made in normal Ringer's solution from visually identified L2/3 pyramidal neurons in D-barrel columns at 30 °C. Miniature excitatory postsynaptic currents were recorded in voltage clamp using Cs gluconate internal (108 mM D-gluconic acid, 108 mM CsOH, 20 mM Hepes, 5 mM TEACl, 2.8 mM NaCl, 0.3 mM EGTA, 4 mM MgATP, 0.3 mM NaGTP, 5 mM BAPTA, pH 7.20, 290 mOsm). Vhold was −90 mV. Cells were excluded if Vrest was >−55 mV or Rseries was >15 MΩ. At least 200 miniature excitatory postsynaptic currents were required. Passive and spiking properties were measured in current clamp using K gluconate internal (116 mM K gluconate, 20 mM Hepes, 6 mM KCl, 2 mM NaCl, 0.5 mM EGTA, 4 mM MgATP, 0.3 mM NaGTP , 5 mM Na2-phosphocreatine, pH 7.25, 290 mOsm). Cells were excluded if Vrest was >−60 mV or Rseries was >15 MΩ. Rseries was compensated for by bridge balance. Liquid junction potential (10–12 mV) was corrected for all recordings. Rinput was calculated as I–V curve slope for −50, 0, and +50 pA current injections. Ih was measured from Vm sag in response to a −200-pA, 500-ms current injection from Vrest. Sag ratio was quantified as (ΔVm at 480–500 ms)/(ΔVm at 120–140 ms) (Fig. S7*D*). Curves relating firing rate and injected current were calculated from 500-ms current injections. Rheobase was defined as the minimal current that elicited at least one spike on five consecutive sweeps. Spike threshold was identified as the prespike Vm at which the second derivative exceeded 6 SDs above the baseline before current injection. Spike width is full width at one-half height. Afterhyperpolarization was measured during spike trains (like in Fig. 5*C*) as spike threshold − (minimum Vm after the spike).

Statistics. Numbers are mean ± SE or median (25th, 75th percentile). Conductance values were nonnormally distributed and compared by nonparametric tests. The critical significance value was 0.05.

1. Drew PJ, Feldman DE (2009) Intrinsic signal imaging of deprivation-induced contraction of whisker representations in rat somatosensory cortex. *Cereb Cortex* 19(2):331–348.
2. Li L, et al. (2009) Endocannabinoid signaling is required for development and critical period plasticity of the whisker map in somatosensory cortex. *Neuron* 64(4):537–549.
3. Freeman JA, Nicholson C (1975) Experimental optimization of current source-density technique for anuran cerebellum. *J Neurophysiol* 38(2):369–382.
4. Margrie TW, Brecht M, Sakmann B (2002) In vivo, low-resistance, whole-cell recordings from neurons in the anaesthetized and awake mammalian brain. *Pflugers Arch* 444(4): 491–498.
5. Jacob V, Brasier DJ, Erchova I, Feldman D, Shulz DE (2007) Spike timing-dependent synaptic depression in the in vivo barrel cortex of the rat. *J Neurosci* 27(6):1271–1284.
6. Wehr M, Zador AM (2003) Balanced inhibition underlies tuning and sharpens spike timing in auditory cortex. *Nature* 426(6965):442–446.
7. Monier C, Fournier J, Frégnac Y (2008) In vitro and in vivo measures of evoked excitatory and inhibitory conductance dynamics in sensory cortices. *J Neurosci Methods* 169(2):323–365.
8. Allen CB, Celikel T, Feldman DE (2003) Long-term depression induced by sensory deprivation during cortical map plasticity in vivo. *Nat Neurosci* 6(3):291–299.
9. Finnerty GT, Roberts LS, Connors BW (1999) Sensory experience modifies the short-term dynamics of neocortical synapses. *Nature* 400(6742):367–371.

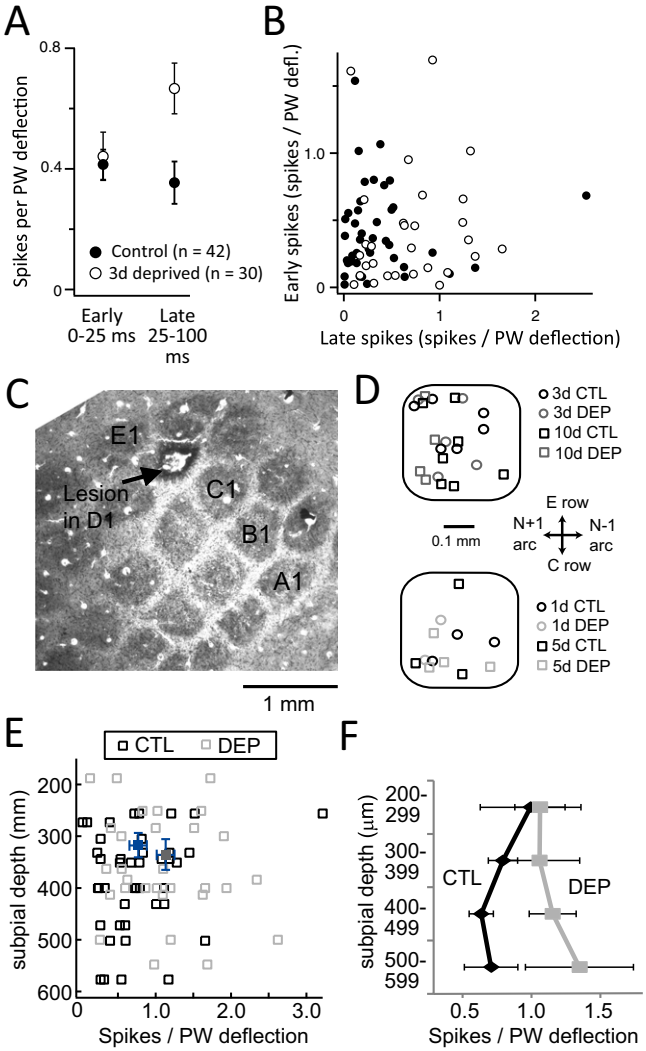

Fig. S1. Additional analysis of single-unit recordings in L2/3. (*A* and *B*) Three-day deprivation selectively increases late spikes in L2/3. (*A*) Mean PW-evoked spike count in early and late poststimulus epochs for 3-d deprived rats and age-matched controls. Bars are SEM. (*B*) PW-evoked spike count in early vs. late windows for each neuron. Late spikes were consistently enhanced in the deprived cell population. (*C–F*) Recording locations for single-unit measurements. (*C*) Example marking lesion recovered in D1 barrel in cytochrome oxidase-stained tangential section through L4 of primary somatosensory in a P24 rat after 3 d of deprivation. (*D*) Reconstructed recording site locations for all penetrations in 1-, 3-, 5-, and 10-d deprived rats and age-matched controls. Locations are plotted relative to normalized barrel boundaries. (*E*) PW response magnitude and recording depth for all L2/3 single units in 3-d deprived rats and age-matched controls. Each symbol is one unit. Mean depth was 387 ± 28 μm for control (CTL) and 366 ± 31 for deprived (DEP) animals ($P = 0.63$, two-tailed t test). (*F*) Mean PW response magnitude for the data in *C* computed in 100-μm depth bins.

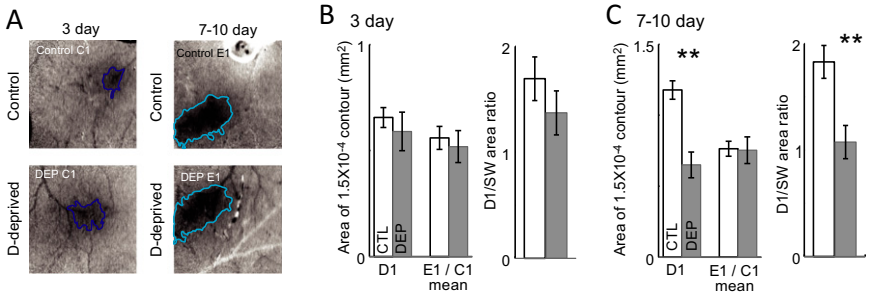

Fig. S2. Comparison of PW and surround whisker (SW) responses in intrinsic signal optical imaging. (*A*) ISOI maps of SW responses for the same imaging fields as in Fig. 2*A*. (*B*, *Left*) Comparison of the D1 whisker area with the mean of E1 and C1 whisker areas for 3-d deprived cases. (*B*, *Right*) Ratio of D1 area to mean E1 and C1 area (SW area) for each individual case. (*C*) Same for 7–10 d of deprivation. $^{**}P < 0.01$.

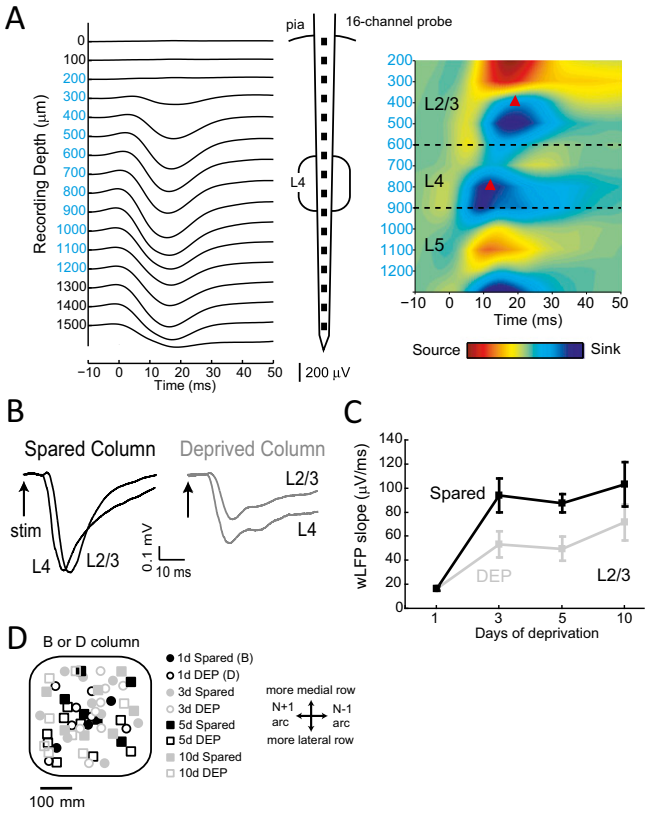

Fig. S3. Reduction of L2/3 whisker-evoked local field potentials (wLFPs) at 3 d of deprivation. (*A*) Raw wLFP traces at (*Left*) different cortical depths measured with (*Center*) a 16-site linear probe. The corresponding current source density plot is shown in *Right*. Dashed lines and barrel outline, approximate layer boundaries. Time 0 is the onset of whisker deflections. The current source density plot reveals separate current sinks in L2/3, L4, and L6a. Red triangles show depths at which L2/3 and L4 wLFPs were measured in plasticity experiments. (*B*) Example wLFPs from L2/3 and L4 of two representative columns in a 3-d deprived rat. (*C*) Effect of deprivation on wLFP slope ratio in L2/3 of deprived and spared columns. (*D*) Recording site locations in wLFP experiments.

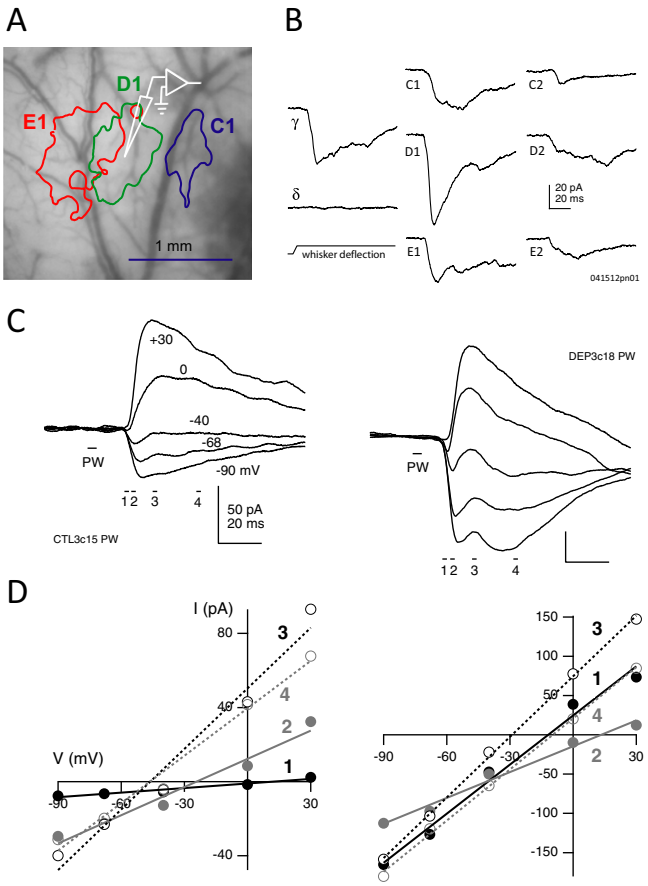

Fig. S4. Whole-cell recording in L2/3 of primary somatosensory in vivo. (*A*) Example of targeting whole-cell recording to D1 functional column based on ISOI. (*B*) Example whisker receptive field measured in voltage clamp (Vhold = −70 mV) from a neuron in the D1 column. Each trace is the mean of 6–20 sweeps. (*C*) wPSCs recorded at several holding potentials in two example cells: *Left*, 3-d control rat; *Right*, 3-d deprived rat. (*D*) I–V plots from the two example cells in *C*. Each symbol type shows the I–V relationship measured at one time window during the synaptic response (windows shown as horizontal lines in *C*).

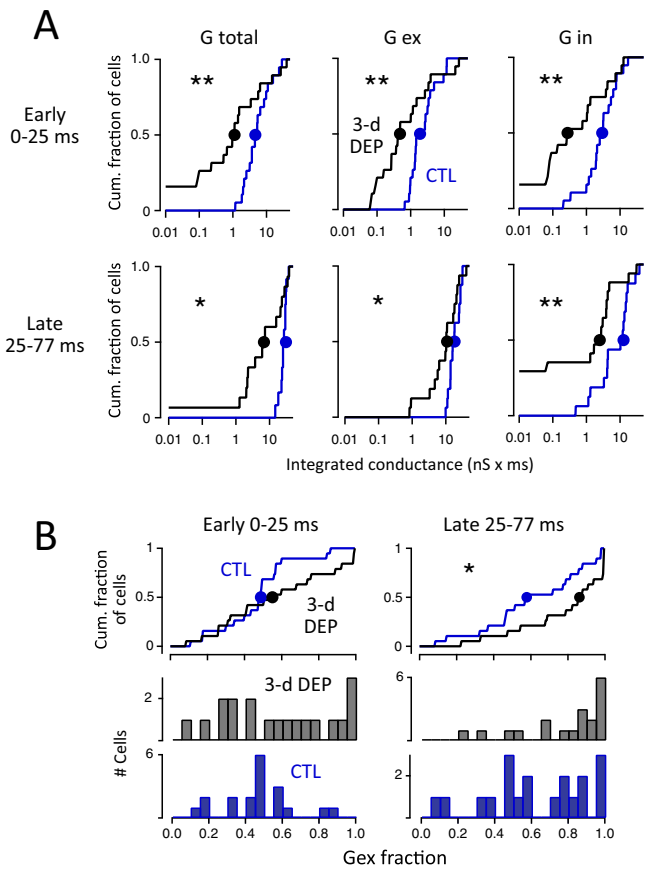

Fig. S5. Effects of 3-d deprivation on early vs. late excitation and inhibition. (*A*) Cumulative histograms of integrated Gtotal, Gex, and Gin in early (0–25 ms) and late (25–77 ms) poststimulus epochs for 3-d deprived and age-matched control cells ($n = 19$ cells each). Circles mark medians. Deprivation significantly reduced each conductance relative to control in both epochs. *$P < 0.05$; **$P < 0.01$, Wilcoxon rank test. (*B*) Histogram and cumulative distributions for Gex fraction for the same cells. Gex fraction was significantly elevated only in the late epoch.

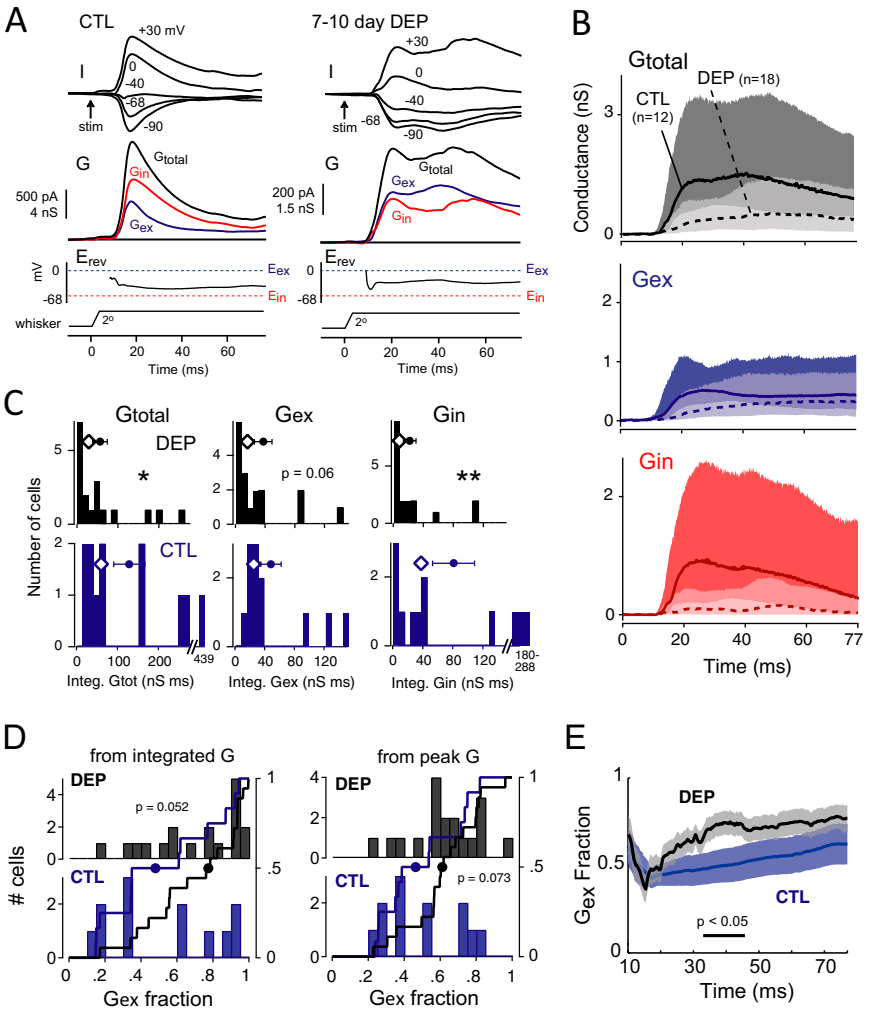

Fig. S6. Disinhibition persists after 7–10 d of deprivation. (*A*) wPSCs and synaptic conductances for two representative cells from (*Left*) a P27 control rat and (*Right*) an age-matched 7-d deprived rat. (*B*) Population Gtotal, Gin, and Gex from 3-d deprived rats and age-matched controls. Lines are median, and shading shows 25th to 75th percentiles. (*C*) Distribution of integrated Gtotal, Gex, and Gin for all cells. Diamonds show median. Circles and bars are mean ± SEM. (*D*) Distribution of Gex fraction calculated from integrated and peak conductance values for each cell. Medians (circles) are marked on cumulative histograms. (*E*) Moment by moment analysis of Gex fraction (1-ms bins) averaged across all cells. Bar indicates time period when Gex fraction was significantly increased in deprived cells by running *t* test.

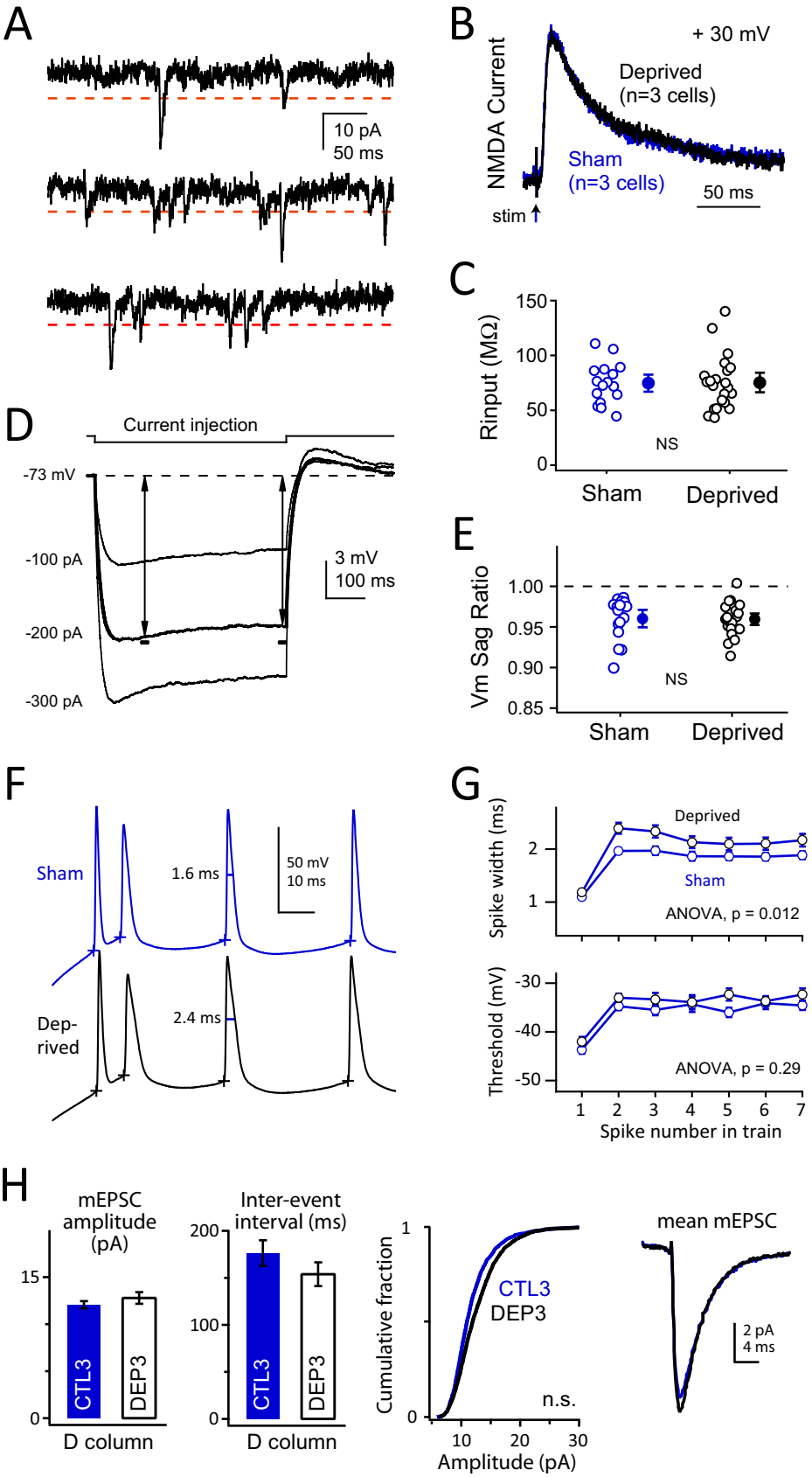

Fig. S7. Three-day deprivation effects on physiology of L2/3 pyramidal cells in ex vivo primary somatosensory slices. (*A*) Example miniature excitatory post-synaptic currents (mEPSCs) from one neuron. Dashed lines show 7 pA mEPSC detection thresholds. (*B*) Deprivation did not alter the kinetics of NMDA-EPSCs

Legend continued on following page

evoked by local stimulation. NMDA-EPSCs were isolated with 10 μM 6,7-dinitroquinoxaline-2,3-dione, 100 μM picrotoxin, and 0.1 mM saclofen and recorded at +30 mV. (*C*) Deprivation did not alter Rinput. Filled circles, mean ± SEM; open circles, individual cells. (*D*) Calculation of Vm sag ratio to measure Ih. Vm sag was blocked by the hyperpolarization-activated cyclic nucleotide-gated channel blocker ZD7288 (20 μM). (*E*) Deprivation did not alter Vm sag ratio. (*F*) Representative spike trains from a sham-deprived cell and a deprived cell in response to current injection (rheobase + 340 pA). Bars, spike width; crosses, spike threshold. (*G*) Effect of 3 d of deprivation on spike width and spike threshold measured for spike trains evoked by rheobase + 340 pA current injection (mean ± SEM; $n = 13$ sham cells, $n = 12$ deprived cells). (*H*) Lack of synaptic scaling for mEPSCs recorded at 22–25 °C. (*Left*) mEPSC amplitude and interevent interval in 3-d deprived rats ($n = 9$ cells) and age-matched controls ($n = 10$). Neither amplitude nor interevent interval was altered by deprivation ($P = 0.33$ and $P = 0.46$, respectively). (*Right*) Mean mEPSCs across all neurons. NS, not significant.

Table S1. Recording characteristics for in vivo whole-cell recordings

Condition	Cells	Depth (μm)	Rseries (MΩ)	Rinput (MΩ)
CTL P23–P25	19	381 ± 19	13.8 ± 1.1	55.7 ± 5.1
DEP 3 d (P23–P25)	19	419 ± 17 ($P = 0.25$)	12.4 ± 0.7 ($P = 0.59$)	56.1 ± 3.5 ($P = 0.30$)
CTL P27–P32	12	388 ± 23	10.4 ± 2.0	44.9 ± 5.6
DEP 7–10 d (P27–P32)	18	381 ± 13 ($P = 0.79$)	9.6 ± 1.2 ($P = 0.71$)	41.6 ± 3.8 ($P = 0.62$)

P values compare deprived with age-matched control condition using a two-tailed *t* test.